Binding of Correolide to the $K_v1.3$ Potassium Channel: Characterization of the Binding Domain by Site-Directed Mutagenesis†

Markus Hanner,‡,§ Brian Green,‡,§ Ying-Duo Gao,§,|| William A. Schmalhofer,‡ Mary Matyskiela,‡ Daniel J. Durand,‡ John P. Felix,‡ Ana-Rosa Linde,‡ Carmen Bordallo,‡ Gregory J. Kaczorowski,‡ Martin Kohler,‡ and Maria L. Garcia*,‡

Department of Ion Channels, and Molecular Systems, Merck Research Laboratories, PO Box 2000, Rahway, New Jersey 07065

Received June 6, 2001; Revised Manuscript Received July 31, 2001

ABSTRACT: Correolide is a novel immunosuppressant that inhibits the voltage-gated potassium channel $K_v1.3$ [Felix et al. (1999) *Biochemistry 38,* 4922−4930]. [^{3}H]Dihydrocorreolide (diTC) binds with high affinity to membranes expressing homotetrameric $K_v1.3$ channels, and high affinity diTC binding can be conferred to the diTC-insensitive channel, $K_v3.2$, after substitution of three nonconserved residues in S_5 and S_6 with the corresponding amino acids present in $K_v1.3$ [Hanner et al. (1999) *J. Biol. Chem. 274,* 25237−25244]. Site-directed mutagenesis along S_5 and S_6 of $K_v1.3$ was employed to identify those residues that contribute to high affinity binding of diTC. Binding of monoiodotyrosine-$HgTX_1$A19Y/Y37F ([^{125}I]$HgTX_1$A19Y/Y37F) in the external vestibule of the channel was used to characterize each mutant for both tetrameric channel formation and levels of channel expression. Substitutions at Leu^{346} and Leu^{353} in S_5, and Ala^{413}, Val^{417}, Ala^{421}, Pro^{423}, and Val^{424} in S_6, cause the most dramatic effect on diTC binding to $K_v1.3$. Some of the critical residues in S_6 appear to be present in a region of the protein that alters its conformation during channel gating. Molecular modeling of the S_5-S_6 region of $K_v1.3$ using the X-ray coordinates of the KcsA channel, and other experimental constraints, yield a template that can be used to dock diTC in the channel. DiTC appears to bind in the water-filled cavity below the selectivity filter to a hydrophobic pocket contributed by the side chains of specific residues. High affinity binding is predicted to be determined by the complementary shape between the bowl-shape of the cavity and the shape of the ligand. The conformational change that occurs in this region of the protein during channel gating may explain the state-dependent interaction of diTC with $K_v1.3$.

Voltage-gated potassium channels play a critical role in the process of human T cell activation (*1*, *2*). These channels have been characterized as $K_v1.3$ homotetramers and shown to control the resting potential of human T cells (*3*, *4*). In the presence of $K_v1.3$ inhibitors, T cells depolarize, and this depolarization attenuates the rise in intracellular Ca^{2+} concentration necessary for T cell activation (*5*). Peptidyl blockers of $K_v1.3$ such as charybdotoxin (*6*), margatoxin (MgTX)[1] (*7*), and *Stichodactyla helianthus* toxin (*8*), inhibit human T cell proliferation in in vitro protocols, and both MgTX (*7*) and kaliotoxin (*9*) display immunosuppressant activity in vivo. Thus, $K_v1.3$ appears to be a novel target for immunosuppression. Because peptides are not ideal candidates for drug development, the search for small molecules that selectively target $K_v1.3$, and that mimic MgTX in in vitro immunological assays has been undertaken. One of these agents, a novel nortriterpene, correolide, has been isolated from the plant *Spachea correa* and shown to be a potent $K_v1.3$ blocker (*10*−*12*). Correolide appears to bind to a site in $K_v1.3$ that is accessible from the intracellular side of the channel, and preferentially blocks open or inactivated channel states (*13*, *14*). In in vitro immunological assays with human T cells, correolide attenuates the Ca^{2+} response, inhibits the Ca^{2+}-dependent pathway of Il-2 production and suppresses, in a reversible fashion, T cell proliferation (*14*). Two analogues of correolide with appropriate pharmacokinetic properties suppress the delayed-type hypersensitivity response to tuberculin in the miniswine (*14*). These data indicate that correolide and its derivatives represent novel immunosuppressant agents.

Correolide binds in a 1:1 stoichiometry with $K_v1.3$ and is a selective inhibitor of the K_v1 family of potassium channels; it does not interact with K_v3 or K_v4 channels, and it is 20-fold weaker against $K_v2.1$ (*10*). It has been possible to confer correolide sensitivity, as measured by [^{3}H]dihydrocorreolide (diTC) binding, to the diTC-insensitive channel, $K_v3.2$, by transferring the S_5-S_6 region of $K_v1.3$, suggesting that this region of the channel contains the receptor site for diTC (*15*). In addition, mutations in a small number of nonconserved residues in the S_5 and S_6 domains of $K_v1.3$ and $K_v3.2$

† M.H. was a recipient of Erwin Schroedinger Fellowships J-01108-MED, and J-01460-MED of the Austrian Research Foundation. Present address: INTERCELL, Rennweg 95B. A-1030 Wien, Austria.

* To whom correspondence should be addressed. Phone: (732) 594-7564. Fax: (732) 594-3925. E-mail: maria_garcia@merck.com

‡ Department of Ion Channels.

§ These authors contributed equally to this work.

|| Department of Molecular Systems.

[1] Abbreviations: K_v, voltage-gated potassium channel; diTC, ditritiocorreolide; diHC, dihydrocorreolide; [^{125}I]$HgTX_1$A19Y/Y37F, monoiodotyrosine-hongotoxin$_1$-A19Y/Y37F; K_d, equilibrium dissociation constant; K_i, equilibrium inhibition constant; k_{-1}, dissociation rate constant; NOE, nuclear Overhauser effect; FLOG, flexible ligands oriented on grid.

10.1021/bi0111698 CCC: $20.00 © 2001 American Chemical Society
Published on Web 09/01/2001

indicated that the lack of sensitivity of $K_v3.2$ to diTC appears to be due to the presence of Phe^{382} and Ile^{387} in S_5, and Met^{458} in S_6 of $K_v3.2$ (residues 346, 351, and 422, respectively, in $K_v1.3$) (*15*). Although all K_v1 series channels display conserved residues in the S_5 and S_6 domains, and diTC binds with similar affinity to all of these channels, the kinetics of ligand binding correlate with the ease by which these channels enter the C-type inactivated state; i.e., diTC association and dissociation is most rapid with $K_v1.3$ and $K_v1.4$ (*15*). In addition, mutations at either of two extracellular vestibule residues of $K_v1.3$ (Gly^{375} and His^{399}) alter kinetics of C-type inactivation (*16*, *17*), and there is a good correlation between the changes in rates of C-type inactivation and the kinetics of diTC binding to these channels (*17*). These findings indicate a state-dependent interaction of correolide with K_v1 channels that, together with the kinetics of binding, may explain the efficacy and limited toxicity of these compounds in vivo.

In the present study, site-directed mutagenesis along S_5 and S_6 of $K_v1.3$ was carried out to identify those residues that contribute to high affinity interaction of diTC with the channel. Substitutions at Leu^{346} and Leu^{353} in S_5, and Ala^{413}, Val^{417}, Ala^{421}, Pro^{423}, and Val^{424} in S_6, cause the most dramatic effect on diTC binding. Molecular modeling of the S_5-S_6 region of $K_v1.3$ predicts that the binding domain for diTC exists in the large water filled cavity that is located below the selectivity filter and that high affinity interaction of the ligand is likely to be due to the existence of a complementary shape between the bowl-shape cavity contributed by the side chains of specific residues and the shape of diTC. The conformational change that occurs in this region of the protein when the channel undergoes transitions to the open/inactivated state may explain the state-dependent interaction of diTC with $K_v1.3$.

EXPERIMENTAL PROCEDURES

Materials. Restriction enzymes and the pCI-neo vector were bought from Promega. The pEGFP-N1 vector was from Clontech, and *Pfu* DNA polymerase from Stratagene. TsA-201 cell line, a subclone of the human embryonic kidney cell line HEK293 that expresses the SV40 T antigen, was a gift of Dr. Robert DuBridge. All tissue culture media were from Gibco, serum was from Hyclone, and the FuGENE6 transfection reagent was from Boehringer Mannheim. HEK293 cells stably transfected with homotetrameric $K_v1.3$ channels were obtained from Professor Olaf Pongs (Zentrum für Molekulare Neurobiologie, Hamburg, Germany). Correolide, diTC (29 Ci/mmol), and dihydrocorreolide (diHC) were prepared as previously described (*10*). Hongotoxin$_1$-A19Y/Y37F ($HgTX_1$A19Y/Y37F) was prepared and radioiodinated as described (*18*). GF/C glass fiber filters were obtained from Whatman, and polyethylenimine was from Sigma. All other reagents were obtained from commercial sources and were of the highest purity commercially available.

Mutant Channel Constructs. A 9E10 c-myc tag was introduced at the C-terminus of $K_v1.3$ using an oligonucleotide cassette containing a *Hin*dIII and *Not*I restriction site. Site-directed mutagenesis was performed using the "overlap extension" technique (*19*). Polymerase chain reaction was carried out using proofreading *Pfu* DNA polymerase and the integrity of all constructs was verified by nucleotide sequencing (automated sequencer, ABI 377).

Transfection of TsA-201 Cells and Membrane Preparation. The procedures for handling TsA-201 cells, their transfection with FuGENE6 transfection reagent, and preparation of membrane vesicles have been previously described (*20*). The final membrane pellet was resuspended in 100 mM NaCl, 20 mM Hepes-NaOH, pH 7.4. Aliquots were frozen in liquid N_2 and stored at −70 °C.

[^{125}I]HgTX$_1$A19Y/Y37F Binding. The interaction of [^{125}I]$HgTX_1$A19Y/Y37F with TsA-201 membranes was measured in a medium consisting of 50 mM NaCl, 5 mM KCl, 20 mM Tris-HCl, pH 7.4, 0.1% bovine serum albumin. For saturation experiments, membranes were incubated with fifteen increasing concentrations of [^{125}I]$HgTX_1$-A19Y/Y37F, in a total volume of 4 mL, for 20 h at room temperature. In each case, the protein concentration in the assay was adjusted to yield a binding signal similar to that of wild-type $K_v1.3$, and triplicate samples were run for each experimental point. Separation of bound from free ligand was achieved using filtration protocols as described (*18*). K_d and B_{max} values for membranes expressing wild-type $K_v1.3$ channels are 0.21 ± 0.05 pM and 1 ± 0.47 pmol/mg of protein, respectively ($n = 12$). B_{max} values for each mutant were compared to the average value of wild-type $K_v1.3$ (1 pmol/mg of protein), expressed as percent control, and averaged. K_d values for mutants were compared to that of wild-type $K_v1.3$ which was always included as a control in each individual determination. The ratios $K_d$mut/K_dWT from individual determinations were averaged. Mutants with no detectable levels of [^{125}I]$HgTX_1$-A19Y/Y37F binding (Figure 1, and Tables 1 and 2) correspond to levels of channel expression <3000-fold than those observed with wild-type $K_v1.3$.

DiTC Binding. Binding of diTC to membranes was carried out in a medium consisting of 135 mM NaCl, 4.6 mM KCl, 20 mM Tris-HCl, pH 7.4, and 0.02% bovine serum albumin. For saturation experiments, membranes were incubated in a total volume of 0.2 mL with increasing concentrations of diTC for 20 h at room temperature. Dissociation kinetics were initiated by addition of 10 μM dihydrocorreolide (diHC) to membrane-bound diTC followed by incubation at room temperature for different periods of time. Competition experiments were carried out in a total volume of 1 mL with 1 nM diTC, in the absence or presence of increasing concentrations of diHC. Under these conditions, IC_{50} values of inhibition are very close to K_i values, since the concentration of diTC in the incubation assay is, at least, 5-fold below K_d. In each case, the protein concentration in the assay was adjusted to yield a binding signal similar to that of wild-type $K_v1.3$. Separation of bound from free ligand was achieved using a filtration protocol as described (*10*, *15*). Thirteen different concentrations of diHC were used in these experiments, and triplicate samples were measured for each experimental point. The data were averaged, and standard deviation of the mean was typically less than 5%. The mean K_i value for diHC in wild-type $K_v1.3$ membranes is 4.9 ± 1.3 nM ($n = 25$). K_i values for mutants were compared to that of wild-type $K_v1.3$ which was always included as a control in each individual determination. The ratios $K_i$mut/K_iWT from individual determinations were averaged. Mutants with no detectable diTC binding (Figure 1 and Tables 1 and 2) correspond to binding levels <100-fold than those observed with wild-type $K_v1.3$.

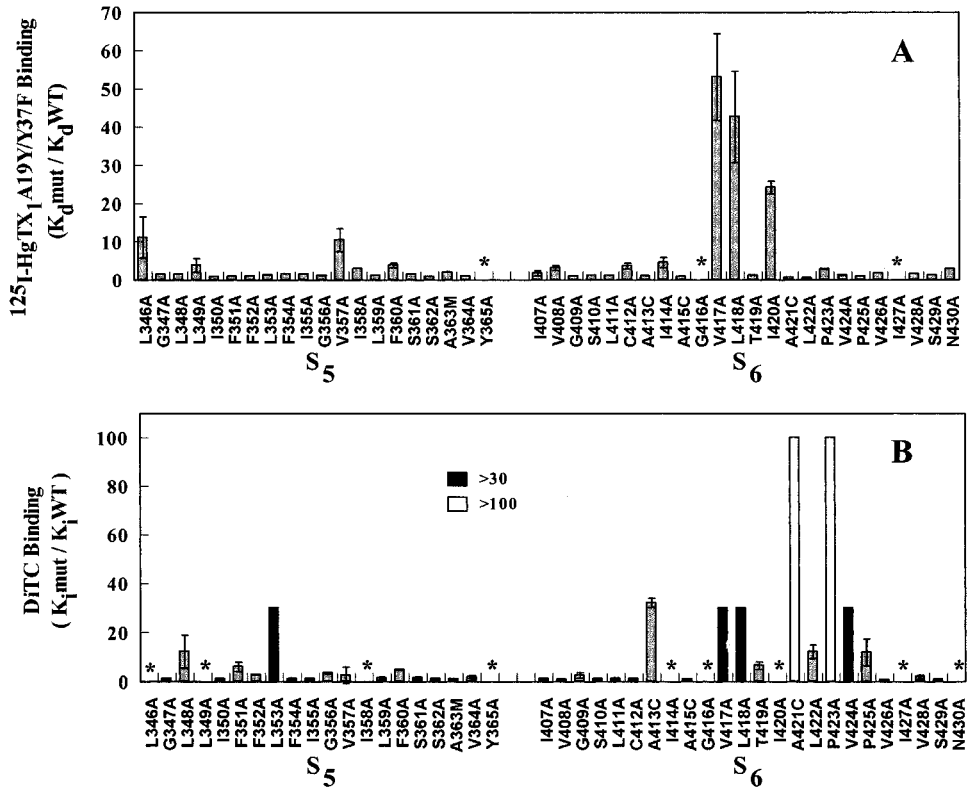

FIGURE 1: Alanine-scanning mutagenesis of $K_v1.3$. (A) Membranes prepared from TsA-201 cells transiently transfected with the indicated mutant were incubated with increasing concentrations of [^{125}I]HgTX$_1$A19Y/Y37F until equilibrium was achieved. Other experimental conditions are given in the Experimental Procedures. Data are presented as the ratio of K_d values for mutant and wild-type $K_v1.3$ versus the corresponding residue mutated. (B) The same membranes as above were incubated with 1 nM diTC in the absence or presence of increasing concentrations of diHC until equilibrium was achieved. Data are presented as the ratio of K_i values for mutant and wild-type $K_v1.3$ versus the corresponding residue mutated. In both A and B, data represent the mean ± SE of two to four determinations with membranes prepared from at least two different transfection experiments. Black and white bars indicate those mutations for which diTC binding was not detected, and the minimum change in diTC affinity (30 and 100-fold, for black and white, respectively) was estimated from the levels of [^{125}I]HgTX$_1$-A19Y/Y37F receptors. Asterisks in panels A and B identify those mutations that do not exhibit either [^{125}I]HgTX$_1$A19Y/Y37F or diTC binding. All residues were mutated to Ala, with the exception of Ala^{363}Met (S_5), and Ala^{413}Cys, Ala^{415}Cys, and Ala^{421}Cys (S_6).

Data Analysis. Data from saturation, ligand association and dissociation experiments were analyzed as described (*15*). IC_{50} values for diHC inhibition were determined using the equation: $B_{eq} = (B_{max} - B_{min})/[1 + (I/IC_{50})^{nH}] + B_{min}$, where B_{eq} is the degree of binding at the ligand concentration tested with no inhibitors present, B_{min} is the minimum amount of ligand bound at higher concentrations of inhibitor where the binding curve has leveled off, I is the inhibitor concentration, nH the Hill coefficient, and IC_{50}, the inhibition constant. For the data presented, B_{max} was usually around 100% and B_{min} was 0%. The change in free energy of diTC binding ($\Delta\Delta G$) was calculated for each mutant according to $\Delta\Delta G = -RT \ln(K_i\text{mut}/K_i\text{WT})$, where R is the gas constant, T is temperature in kelvin, and K_i is the equilibrium inhibition constant.

Molecular Modeling. A $K_v1.3$ homology model was generated using the Modeler module with InsightII (MSI), and the KcsA structure (1BL8) as a template. Sequence alignments between KcsA and K_v channels are as indicated (*21*). In the model, slight differences were observed in the S_5 loop region (outer loop) of $K_v1.3$. This model is called the straight $K_v1.3$ model in the following discussions.

The most challenging part in modeling the $K_v1.3$ channel concerned the carboxyl one-third end of the S_6 helix, where the PVP sequence is present. These two almost adjacent proline residues could bend the α-helix in various directions (*22*, *23*). In addition, the S_5 helix could also be affected if bending of S_6 takes place. Interestingly, Gly^{347} in S_5 lies at the same level as the PVP region. Like proline, glycine is another putative α-helix breaker, and may also be associated with helix packing (*24*). Thus, Gly^{347} could cause a slight kink in S_5 to accommodate the bend of the S_6 helix. To define all these features in our $K_v1.3$ model, the following steps were carried out:

1. The S_5 helix from residues Lys^{340} to Gly^{347} was intentionally rotated away from the S_6 helix to allow a fully thorough sampling of S_6.

2. To derive a diverse ensemble of conformations for a PVP region that behaves as a flexible linker between two helices, the torsion angles belonging to the backbone and side chains of the Pro^{423}−Val^{424}−Pro^{425} region, and those belonging to the side chains of residues between Val^{426} and Arg^{437} were set free, while all remaining torsions, bond lengths and bond angles were fixed. With these constraints, a knowledge-based sampling of the torsion subspace was carried out to generate 200 diverse conformations (*25*). Then four copies of each structure were made, and superimposed on the four subunits of the $K_v1.3$ tetramer model.

3. As suggested from experimental data for *Shaker* (*26*), the distances between Val^{426} of one subunit (I) and His^{436} of its neighbor subunit (I′) should be about 5.2−10 and 3.8 Å, for Cα atoms and side chains, respectively (*27*). These values were then used as the only criteria for choosing a final structure from the 200 conformation set.

Table 1

	S_5			S_6	
	[^{125}I]HgTX binding (% control)	$\Delta\Delta G$ diTC (kcal/mol)		[^{125}I]HgTX binding (% control)	$\Delta\Delta G$ diTC (kcal/mol)
L346A	3 ± 1*	ND	I407A	43 ± 24	0.11
G347A	78 ± 32	0.11	V408A	42 ± 5	−0.10
L348A	60 ± 29	1.47	G409A	68 ± 42	0.50
L349A	9 ± 4*	ND	S410A	141 ± 67	0.06
I350A	45 ± 9	0.06	L411A	73 ± 10	0.08
F351A	10 ± 1	1.06	C412A	91 ± 61	0.08
F352A	44 ± 24	0.61	A413C	164 ± 11	2.03
L353A	43 ± 18	>1.99	I414A	6 ± 2*	ND
F354A	116 ± 28	0.06	A415C	123 ± 42	−0.03
I355A	13 ± 10	0.09	G416A	ND*	ND
G356A	61 ± 35	0.73	V417A	18 ± 11	>1.99
V357A	25 ± 1	0.63	L418A	25 ± 3	>1.99
I358A	4 ± 3*	ND	T419A	65 ± 26	1.10
L359A	25 ± 5	0.22	I420A	4 ± 1*	ND
F360A	44 ± 4	0.93	A421C	111 ± 20	>2.7
S361A	83 ± 44	0.25	L422A	43 ± 15	1.38
S362A	45 ± 2	0.07	P423A	121 ± 17	>2.7
A363M	180 ± 48	0.06	V424A	25 ± 7	>1.99
V364A	47 ± 16	0.39	P425A	184 ± 127	1.46
Y365A	ND*	ND	V426A	136 ± 60	−0.17
			I427A	ND*	ND
			V428A	104 ± 36	0.28
			S429A	76 ± 5	−0.13
			N430A	1 ± 1*	ND

[a] The maximum number of [^{125}I]HgTX$_1$-A19Y/Y37F receptors was determined as described in the text. Values represent the average of two to four determinations carried out with different membrane preparations. $\Delta\Delta G$ values for diTC binding were calculated as described. ND; not detected. (*) Expression levels <10% those of wild-type K_v1.3.

Table 2[a]

	[^{125}I]HgTX binding (% control)	diTC binding (K_i mut/K_i WT)	$\Delta\Delta G$ diTC (kcal/mol)
L346F	58 ± 11	25 ± 3.1	1.89
A413S	60 ± 14	2.9 ± 0.14	0.62
A413T	46 ± 14	2.5 ± 1.36	0.54
G416C	ND	ND	
V417C	20 ± 15	43 ± 8	2.20
I420C	30 ± 21	ND	
A421S	40 ± 21	1.9 ± 1.4	0.38
P423C	102 ± 10	1.2 ± 0.20	0.11
P423I	551 ± 91	4.5 ± 2.6	0.88
P423N	9 ± 1	4.8 ± 2.8	0.92
P423Q	16 ± 8	12 ± 2.82	1.46
P423S	4 ± 1	ND	
P423T	78 ± 23	1.4 ± 0.60	0.20
P423W	109 ± 1	16.5 ± 4.94	1.64
V424C	28 ± 12	ND	
V424I	694 ± 168	2.6	0.56
I427C	2 ± 1	ND	

[a] [^{125}I]HgTX$_1$-A19Y/Y37F and diTC binding were determined as described in the text. Values represent the average of two to four determinations carried out with different membrane preparations. $\Delta\Delta G$ values were calculated as described. ND; not detected.

4. Because the bend of the S_6 helix at PVP may affect the S_5 conformation through helical interactions, the S_5 helix was sampled at the Glu^{345} to Gly^{347} torsion subspace using the same method as described for the PVP region, after the S_6 conformation had been chosen. The criteria for selecting the S_5 conformation were (a) it should not collide with the S_6 helix; (b) it should remain as close as possible to S_5 in the KcsA structure; as long as the van der Waals contacts permit, S_5 and S_6 should have maximal packing contact, as they appear in the KcsA structure.

5. The final structure was energy minimized using the distances between four pairs of Cα atoms of Val^{426}(I) and His^{436}(I′) as NOE constraints. In the minimization, the backbone of residues between Leu^{348} and Leu^{422} was completely fixed. For those residues located between Lys^{340} and Gly^{347} at the beginning of S_5, and Pro^{423} and Arg^{437} in the carboxyl end of S_6, the side chains were first minimized 2000 steps in order to remove side chain close contacts, and then the backbone was also released and minimized for 15 000 steps. The minimization calculations were carried out with the program CHARMM (*28*) using the MMFFs force field (*29*). This model will be referred as the bent K_v1.3 model in following discussions.

To dock diTC in the bent model of the K_v1.3 channel, 100 low energy conformations of the molecule were generated using distance geometry (*25*, *30*), and energy minimized using the MMFFs force field. The molecule was then docked using the FLOG (Flexible Ligands Oriented on Grid) procedure (*31*). The average RMSD value for the minimized conformational set is 1.2 Å, with maximum and minimum values of 3.4 and 0.48 Å, respectively.

RESULTS

Alanine-Scanning Mutagenesis of K_v1.3 (S_5, S_6). Previous studies employing chimeras between K_v1.3 and the diTC-insensitive channel, K_v3.2, have identified Leu^{346} and Phe^{351} in S_5 and Leu^{422} in S_6 of K_v1.3 as being important for diTC binding (*15*). In this study, we have extended our analysis by first performing an alanine scan of these three residues and their neighbors in S_5 and S_6. At those positions where alanine is the amino acid present in the wild-type channel, methionine (363 in S_5) or cysteine (413, 415, 421, S_6) substitutions were used. These later substitutions were chosen because of the presence of such a residue at the equivalent position in other diTC-insensitive K_v channels (*15*) or because

of the reported tolerability of the substitution for maintaining channel function (*32*, *33*). Individual $K_v1.3$ mutants were transiently expressed in TsA-201 cells, and membranes were prepared. Constructs were initially analyzed for tetrameric channel assembly, and levels of channel expression by determining the binding characteristics of monoiodotyrosine-$HgTX_1$A19Y/Y37F ([^{125}I]$HgTX_1$A19Y/Y37F) to these membranes. This is important for two reasons. First, when a large effect on diTC binding is observed, it is necessary to eliminate the possibility of there being severe lack of protein expression. Second, it was reasoned that mutations along the transmembrane domains should not have a pronounced effect on the interaction of [^{125}I]$HgTX_1$A19Y/Y37F with the external vestibule of the channel. Thus, large effects on ligand affinity in this binding interaction were interpreted to mean that the tetrameric subunit assembly was compromised by the introduced mutation and that a global conformational change in the protein had taken place. In general, levels of expression for a large number of mutants, as determined from the maximum number of [^{125}I]$HgTX_1$A19Y/Y37F binding sites, were within 10-fold of those seen with wild-type $K_v1.3$ (Table 1). There are, however, a few exceptions. The channel mutants Leu^{346}Ala, Leu^{349}Ala, Phe^{351}Ala, and Ile^{358}Ala in S_5, and Ile^{414}Ala, Ile^{420}Ala, and Asn^{430}Ala in S_6 yielded expression levels that were 10% or less than those of the wild-type channel. In addition, alanine substitutions at Tyr^{365} in S_5, and Gly^{416} and Ile^{427} in S_6 gave no detectable levels of channel expression. The reason(s) for the lowest expression of these mutants has not been investigated. It is possible that the mutated residue plays a key role in early folding events and that the kinetics of this process are altered by the mutation. Although for some residues alanine substitution can alter significantly the amount of channel expression, other substitutions at these positions are better tolerated (*15*); see also Table 2. Importantly, the characteristics of [^{125}I]$HgTX_1$A19Y/Y37F binding to membranes are similar to those found when [^{125}I]$HgTX_1$A19Y/Y37F binding was monitored to intact cells after transient transfection with the corresponding cDNAs of S_6 mutants (the K_d for peptide is equivalent and the B_{max} is proportionally changed, data not shown). Under these conditions, [^{125}I]$HgTX_1$A19Y/Y37F only binds to channels expressed at the cell surface. The consequences of alanine mutagenesis on the affinity of [^{125}I]$HgTX_1$A19Y/Y37F to these channels are illustrated in Figure 1A. In this plot, a ratio of 1 represents identical behavior for mutant and wild type, whereas a ratio of >1 indicates a decrease in ligand affinity as a result of the amino acid substitution. Most mutations in S_5, with the exception of Val^{357}Ala, had no significant effect on the peptide's affinity for the channel. In marked contrast, each of three positions in S_6, Val^{417}Ala, Leu^{418}Ala, and Ile^{420}Ala, causes a large destabilization in the interaction of [^{125}I]$HgTX_1$A19Y/Y37F with the channel's vestibule. These data indicate that the overall conformation of the protein appears to be altered in these mutants.

Binding of diTC to $K_v1.3$ Mutants. To determine the consequences of these mutations on diTC binding, channel mutants were characterized as described under Experimental Procedures. Results of these experiments are presented in Figure 1B and Table 1. For a large number of mutants, binding of diTC was consistently observed, and in these cases, data are presented as the mean ± SE of determinations from at least two different transfection experiments. In other cases, levels of channel expression and diTC binding were very low or undetectable, and the effect of mutating the residue could not be accurately assessed, given the low specific activity (~28 Ci/mmol) of diTC. These positions are identified by an asterisk. Positions displayed in white or black indicate those residues that yield good levels of channel expression, but no detectable diTC binding. In these cases, the relative change in ligand affinity (>30, black; >100, white), can only be estimated from the maximum levels of [^{125}I]$HgTX_1$A19Y/Y37F binding. Given these considerations, the most significant effects on diTC binding are observed for the mutations Leu^{353}Ala in S_5, and Ala^{413}Cys, Ala^{421}Cys, Pro^{423}Ala, and Val^{424}Ala in S_6. The change in the free energy of the binding reaction ($\Delta\Delta G$) for these mutants is >1.5 kcal/mol. Although the levels of channel expression of these mutants, with the exception of Leu^{353}Ala (ca. 43%) and Val^{424}Ala (ca. 25%), are comparable to those observed with wild-type $K_v1.3$, diTC binding can only be detected with the Ala^{413}Cys mutant, but with ~40-fold lower affinity. The estimate for the change in diTC affinity associated with either Ala^{421}Cys or Pro^{423}Ala is >100-fold, whereas for Leu^{353}Ala and Val^{424}Ala it is >30-fold, given the corresponding levels of channel expression. Two other mutants, Val^{417}Ala and Leu^{418}Ala in S_6, are also predicted to have large effects on diTC binding. These mutations, however, may have caused a global conformational change in the protein because [^{125}I]$HgTX_1$A19Y/Y37F binding is also severely affected. Other positions for which an intermediate change in diTC affinity was found are Leu^{348} and Phe^{351} in S_5, and Thr^{419}, Leu^{422}, and Pro^{425} in S_6, with $\Delta\Delta G$ values between 1 and 1.5 kcal/mol. It is interesting to note that several residues of S_6 with $\Delta\Delta G$ values of <1 kcal/mol such as Ile^{407}, Val^{408}, Ser^{410}, Leu^{411}, Ala^{415}, Tre^{419}, Val^{426}, and Ser^{429} are not conserved within voltage-gated potassium channels (*34*).

Other Mutagenesis Studies. The tolerability of specific residues to various substitutions was analyzed in further detail. Because of all experimental evidence suggesting that correolide binds in the internal water filled cavity within the axis of symmetry of the $K_v1.3$ channel (*10*, *13*, *14*, and see below), the residues chosen for these studies were those of S_6 predicted to face the pore that have the largest effect on diTC binding when mutated to Ala (Table 1), such as Ala^{413}, Val^{417}, Ala^{421}, and Val^{424}. In addition, other residues that yield very low levels of expression when mutated to Ala, such as Leu^{346}, Ile^{420}, and Ile^{427}, were mutated to either Phe (Leu^{346}) or Cys because of the reported expression of the respective mutant channel elsewhere (*15*, *32*). Finally, Pro^{423} was also subjected to further analysis because of its large contribution to diTC binding and its critical position as part of the Pro-Val-Pro sequence motif. Results of these experiments are presented in Table 2. In contrast to the situation with the Leu^{346}Ala mutant (Table 1), Leu^{346}Phe, which represents a conserved substitution when compared with other K_v channels, yields levels of expression that are within 2-fold of those seen with wild-type $K_v1.3$. Leu^{346}Phe displays lower affinity for diTC with a $\Delta\Delta G$ value of 1.89 kcal/mol. It is interesting to note that lack of sensitivity of $K_v3.2$ to diTC has been correlated with the presence of Phe at the corresponding 346 (Leu) position of $K_v1.3$ (*15*). Further insight into the consequences of the Leu^{346}Phe mutation has been obtained by determining the kinetics of diTC binding in this mutant.

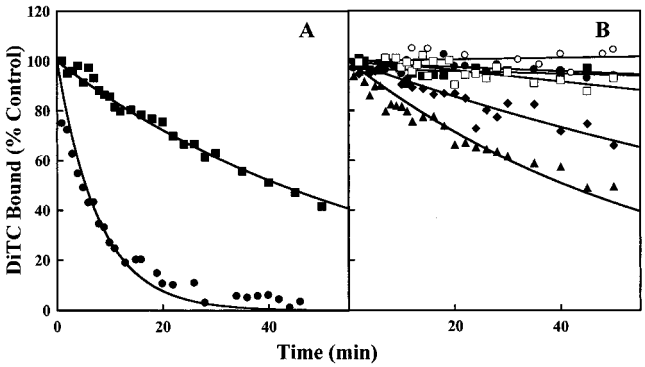

FIGURE 2: Kinetics of binding of diTC to mutant $K_v1.3$ channels. Membranes prepared from TsA-201 cells transiently transfected with either $K_v1.3$ (■), $K_v1.3$/L346F (●) (A), $K_v1.3$/A415C (□), $K_v1.3$/P423C (■), $K_v1.3$/P423I (●), $K_v1.3$/P423T (○), $K_v1.3$/V424I (▲), or $K_v1.3$/P425A (♦) (B), were incubated with 10 nM diTC until equilibrium was achieved. Dissociation kinetics were initiated by addition of 10 μM diHC, followed by incubation at room temperature for different periods of time. Specific binding data have been fit to a single monoexponential decay corresponding to a first-order reaction. (A) (■) k_{-1}= 0.016 min^{-1}; (●) k_{-1}= 0.12 min^{-1}. (B) (▲) k_{-1}= 0.017 min^{-1}; (♦) k_{-1}= 0.008 min^{-1}.

As shown in Figure 2A, dissociation kinetics from $K_v1.3$/Leu^{346}Phe are markedly enhanced ca. 8-fold with respect to the wild-type channel. In fact, most of the change in affinity for this mutant can be accounted for by the increase in the dissociation rate constant of diTC. It appears that the diTC-bound state is highly destabilized in this mutant as a consequence of either a direct contribution of this residue to the binding site or a conformational change propagated to another part of the protein where the ligand binds.

An interesting finding concerns the substitutions at Pro^{423}, a residue that is conserved within voltage-gated potassium channels, predicted to face away from the pore, and when mutated to Ala causes a large effect on diTC binding. Neither Cys, Thr, Ile, nor Asn substitutions at this position have large effects on diTC binding, whereas Gln and Trp mutants display an intermediate sensitivity to diTC. These data suggest that the size of the residue at position 423 may be an important determinant for diTC binding. At position Ala^{421}, Cys substitution largely destabilizes diTC binding. However, Ser substitution at the same position confers a wild-type phenotype, whereas the Ala^{421}Thr mutant does not express tetrameric channels. Although the number of substitutions studied at position 421 is limited, the data appear to be consistent with the idea that the size of the residue plays an important role in diTC binding as found at position 423. At position Val^{424}, an Ile substitution is the only one that yields a wild-type phenotype for diTC binding. This substitution is conserved in the K_v2 channel family. Ala substitutions at positions 417 and 420 yield low levels of channel expression, and Val^{417}Ala channels also display large changes in [^{125}I]HgTX$_1$A19Y/Y37F binding affinity, making it difficult to define the contribution of these residues to diTC binding. Cys substitution at these residues restores both normal levels of expression and wild-type [^{125}I]HgTX$_1$A19Y/Y37F binding properties. These two channels, however, do not bind diTC. Many substitutions at Ala^{413} (Phe, His, Gln, Tyr, Asn, and Trp) do not express tetrameric channels. The only substitutions tolerated at this position appear to be Cys, Thr and Ser (this study) and Val (*35*, *36*). Both Thr and Ser mutants display ca. a 3-fold decrease in affinity for diTC. Lack of expression of Ile^{414}Trp and Ile^{427}Cys, within a *Shaker* channel background, has been previously reported (*32*, *34*).

Because it was not possible to measure diTC kinetic binding parameters with Ala^{421}Cys, Pro^{423}Ala, and Val^{424}Ala mutants, and hence determine which step of the binding reaction was affected, kinetics of diTC dissociation were determined for other mutants that either have decreased ligand affinity (such as Pro^{425}Ala), or display $\Delta\Delta G$ values of <1 kcal/mol (such as Ala^{415}Cys, Pro^{423}Cys, Pro^{423}Ile, Pro^{423}Tre, or Val^{424}Ile). Results of these experiments are presented in Figure 2B. Both Pro^{425}Ala and Val^{424}Ile mutants display kinetics of ligand dissociation (k_{-1} values of 0.008 and 0.017 min^{-1}, respectively) that are not much different from those of the wild-type channel (k_{-1}= 0.016 min^{-1}), despite the different effects of these mutants on diTC binding. However, four other mutants that bind diTC with similar affinity as $K_v1.3$, Ala^{415}Cys, Pro^{423}Cys, Pro^{423}Ile, and Pro^{423}Thr, have a >10-fold reduction in the rate of ligand dissociation. These data indicate that rates of ligand association must also be proportionally affected, and that the lack of binding observed with some of the S_6 mutants could in part be related to limited access of diTC to its binding site.

In earlier studies, the rate of C-type inactivation has been shown to affect the kinetics, but not the affinity, of diTC binding to $K_v1.3$ (*15*, *17*). To eliminate the possibility that the effect of the mutations on diTC binding to $K_v1.3$ could result from changes in the C-type inactivation properties of the altered channel, the same mutations were analyzed against a $K_v1.2$ channel background. This channel displays the same amino acid sequence in S_5 and S_6 as $K_v1.3$, but activates at more depolarized potentials and does not inactivate. The affinities of diTC for $K_v1.2$ and $K_v1.3$ channels are identical, although the kinetics of binding are much slower with $K_v1.2$, due to the absence of C-type inactivation in this channel (*15*). Alanine was substituted in $K_v1.2$ at the equivalent positions of $K_v1.3$, Leu^{422}, Pro^{423}, Val^{424}, Pro^{425}, and Val^{426}, whereas cysteine was substituted at Ala^{413} and Ala^{421}. Equilibrium binding studies of diTC to $K_v1.2$ mutants (data not shown) yield the identical pattern as that observed with $K_v1.3$ (Table 1), suggesting that these residues are most likely involved in ligand binding, and that the effect of the mutations are not due to changes in the biophysical properties of the $K_v1.3$ channel.

Docking DiTC into $K_v1.3$. A molecular model of the S_5-S_6 region of $K_v1.3$ was generated using the crystal structure of the KcsA channel as a template (*21*), and diTC was docked using constraints derived from functional (*10*, *13*, *14*), and mutagenesis experiments (this study). Figure 3 presents the CPK model structure of $K_v1.3$ with either a straight α-helical S_6 (A) or a bent S_6 (B). In these models, the channel vestibule has the same architecture as in a previously reported model of the pore region of the channel (*37*). Residues colored blue or red had $\Delta\Delta G$ values of >1 or >1.5 kcal/mol, respectively, for diTC binding when mutated to alanine. Residues in green had $\Delta\Delta G$ values of <1 kcal/mol, and the purple color indicates residues that cause loss of channel expression when mutated to alanine. Several lines of evidence are consistent with the water-filled cavity beneath the selectivity filter as the region of the channel where diTC binds: (a) correolide's binding site is accessible from the intracellular surface of the channel (*13*, *14*); (b) the stoichiometry of diTC binding is one per channel, suggesting that the binding site must be

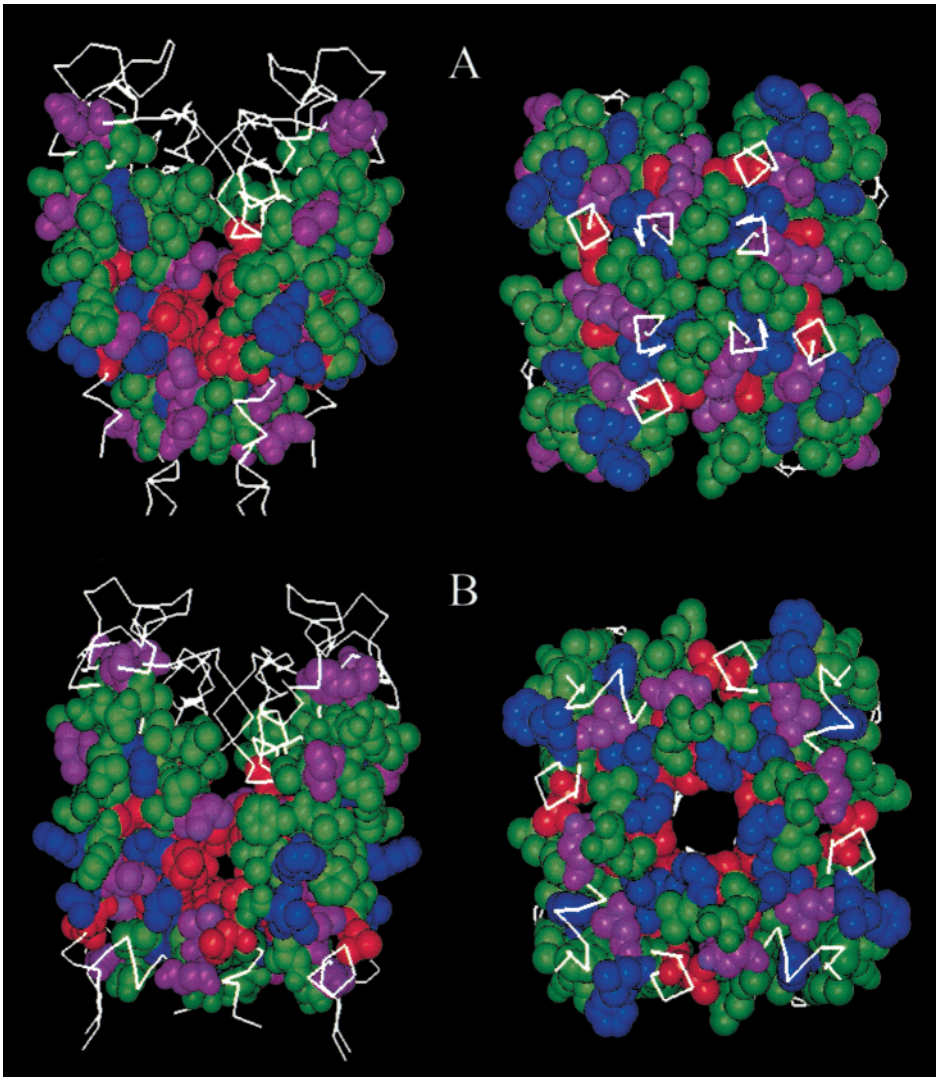

FIGURE 3: CPK model of $K_v1.3$ (S_5-S_6). The model with a straight S_6 helix (A) was generated using the crystal structure of the KcsA channel as a template (*21*). The model with a bent S_6 helix (B) was generated using the crystal structure of the KcsA channel as a template (*21*), and modified as described in the Experimental Procedures. Residues colored blue or red had $\Delta\Delta G$ values >1, or >1.5 kcal/mol, respectively, for diTC binding when mutated to alanine. Residues in green displayed $\Delta\Delta G$ values of <1 kcal/mol for diTC binding, and the purple residues are positions at which no channel expression is detected when mutated to alanine. Both a side (left) and a bottom (right) view of the channel are presented. Note that in panel A, the intracellular entrance to the channel is made up of green residues and it is narrow, whereas in panel B the intracellular entrance is broad and is made up of residues that are important for diTC binding.

located within the channel's center of symmetry (*10*); (c) both verapamil (*38*) and UK-78,282 (*39*), two structurally different types of $K_v1.3$ inhibitors that have previously been postulated to bind within the water-filled cavity, inhibit binding of diTC with K_i values of 2700 and 260 nM, respectively (data not shown). The major differences between the two models in Figure 3 occur at the intracellular entrance to the pore. Only the bent model predicts an entrance wide enough to allow access of diTC to the inner cavity, and it is surrounded by the important residue Val^{424}, the Val in the PVP motif.

The hydrophobic surface of those residues that have the largest effect on diTC binding is illustrated in Figure 4A. It is interesting to note the presence of two major hydrophobic pockets. One covers the surface along the channel wall formed by the S_6 helices (Ala^{413}, Val^{417}, Ala^{421}, and Val^{424}), whereas the other one is present at the interface between the S_5 and S_6 helices, and therefore would be represented four times in a tetrameric channel structure. Docking of diTC yields two possible orientational modes which are energetically indistinguishable. One orientation has the 3-keto group of the E-ring ester pointing to the selectivity filter, with the saturated hydrocarbon side of the molecule interacting with the hydrophobic wall of the channel, and the other side of the molecule, with five acetyl groups, lying in the water-filled cavity. In the second orientation, the ether group of the A-ring lactone points to the selectivity filter, and the rest of the molecule interacts with the channel in a similar fashion as in the first orientation. The structure−activity relationship of correolide can be used to predict the most likely orientation of the molecule in the cavity. First, the structure−activity relationship within the correolide series indicates that addition or removal of H-binding groups, or substitution of hydrophobic groups, does not have a marked effect on $K_v1.3$ blocking activity (*10*, *14*, *40*, *41*), suggesting that the molecule does not make any H-bond interactions with the channel. Second, the decrease in affinity observed after removal of the C-4 acetyl group (*10*) could be the result of eliminating a favorable van der Waals contact with the channel. Third, the C-4 substituted correolide analogues

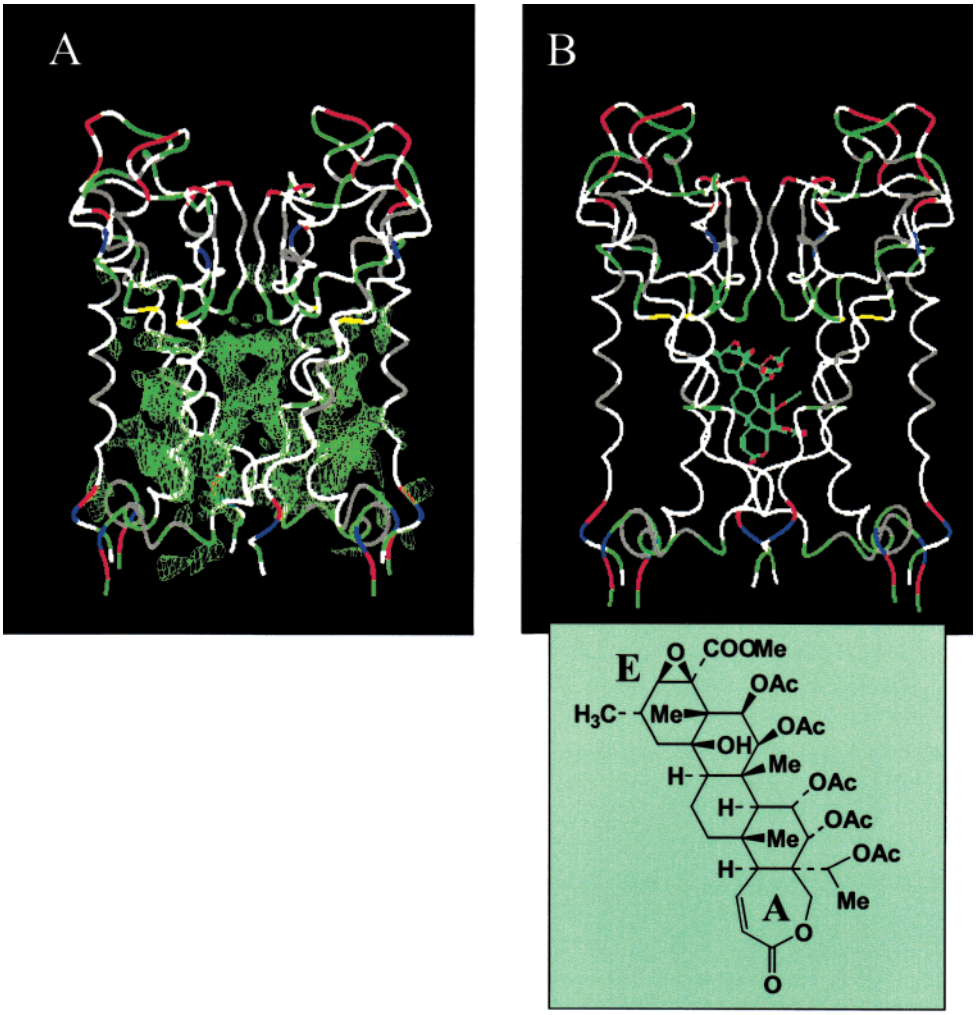

FIGURE 4: Docking of diTC in $K_v1.3$. $K_v1.3$ (S_5-S_6) with a bent S_6 helix is shown. The hydrophobic surface around the cavity of those residues that contribute to diTC binding is presented in green (A). Two major hydrophobic areas are present. One covers the area along the channel wall formed by the S_6 helices and the other represents an area between S_5 and S_6 helices that is present four times in the tetrameric channel. Docking by the FLOG procedure (*31*) shows diTC sitting along the channel wall in one of its two most stable orientations (B). In this orientation, the 3-keto group of the E-ring ester points to the selectivity filter with the saturated hydrocarbon face of the molecule interacting with the hydrophobic wall of the channel, and the other face, with five acetyl groups, lying in the water-filled cavity. In an alternative orientation, the ether group of the A-ring lactone is oriented toward the selectivity filter, and the rest of the molecule interacts with the channel in a similar fashion as above. DiTC does not make any specific H-bond interactions with the channel, and high affinity binding is presumed to be the result of a complementary shape between the bowl-shaped cavity of the channel and the shape of diTC. In both panels A and B, colors represent residues with the following properties: white, hydrophobic; green, polar; red, negatively charged; blue, positively charged; gray, aromatic, yellow, cysteine.

which have been shown to have immunosuppressant activity in vivo (*14*) can be docked so that the 3-keto group of the E-ring ester is proximal to the selectivity filter, while the C-4 benzyl group fits into the bottom of the water-filled cavity and makes contact with the side chains of Val^{424} and Pro^{425}. Perhaps the C-4 benzyl substitution provides binding energy through a van der Waals interaction. This idea suggests that the Mode One orientation of correolide binding described above might be favored. Taken together, these data are consistent with the hypothesis that binding of diTC is determined by the complementary shape between the bowl-shape of the cavity and the shape of the ligand (Figure 4B). This idea is supported by mutagenesis studies of Val^{417}, Ala^{421}, Pro^{423}, and Val^{424}. Thus, polar substitutions at some of these positions are tolerated as long as the shape and size of the cavity remain the same. For instance, Ala^{421}Ser and Ala^{421}Cys display $\Delta\Delta G$ values for diTC binding of 0.38 and >2.7 kcal/mol, respectively. Although Ser is a more polar residue than Cys, the size of its side chain is closer to that of Ala, and it has less effect on diTC binding. Substitutions at Pro^{423} are consistent with the idea that this residue does not interact directly with diTC and affects binding through an allosteric mechanism, by determining the shape of the cavity through its packing with the S_5 helix (Figure 5).

Although two residues in S_5, Leu^{346} and Leu^{353}, had significant effects on diTC binding, this could be the result of a disruption in the helical packing between S_5 and S_6. Figure 5 indicates the position of these two S_5 residues in relation to other important residues of S_6. Leu^{353} appears to have close contacts with Gly^{416} in the same channel subunit, a residue that when mutated to either Ala or Cys does not express channels. Both Leu^{353} and Gly^{416} lie at the same level at the bottom of the selectivity filter, and changes in either residue could affect the selectivity filter and other regions of the pore. The side chains of residues Ile^{427} and Asn^{430} in S_6, and Leu^{346} in S_5, in the same subunit, are facing each

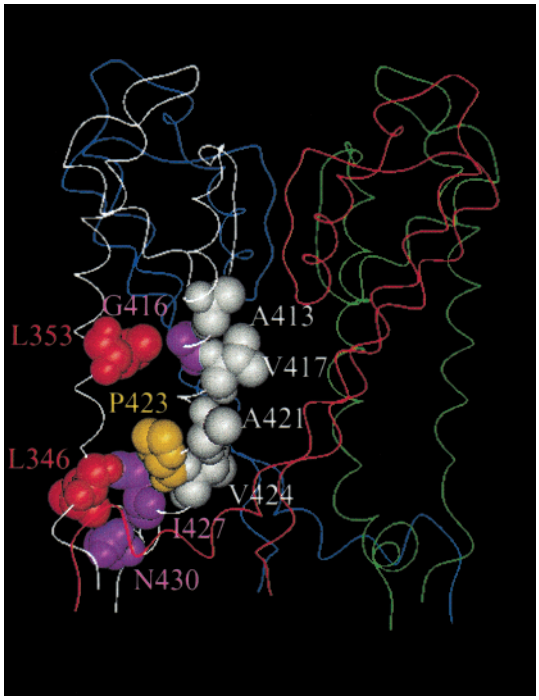

FIGURE 5: Helical packing between S_5 and S_6 in $K_v1.3$. The four $K_v1.3$ (S_5-S_6) subunits with a bent S_6 helix are shown, each in a different color. The side chains of two critical residues of S_5, Leu^{346}, and Leu^{353}, and eight residues of S_6, Ala^{413}, Gly^{416}, Val^{417}, Ala^{421}, Pro^{423}, Val^{424}, Ile^{427}, and Asn^{430}, are illustrated. These residues are all located in the same channel subunit which is depicted in a white color. Residues colored white have their side chains facing the pore, and three of them, Val^{417}, Ala^{421}, and Val^{424} are predicted to directly participate in diTC binding. Leu^{353} appears to have close contacts with Gly^{416} and both residues are located at the same level of the channel, at the bottom of the selectivity filter. The side chains of Leu^{346} are also in close proximity with those of Pro^{423}, Ile^{427}, and Asn^{430}. The effects of substitutions at Pro^{423} on diTC binding can be explained by the contribution of this residue to determining the shape of the cavity through its packing with the S_5 helix. Ile^{427} does not express functional channels when mutated to either alanine (this study), or cysteine (this study, ref *32*), and a tryptophan substitution of *Shaker* at this position has a very pronounced effect on channel gating (*34*).

other closely (Figure 5). It is interesting to note that mutants Ile^{427}Ala(Cys) do not express channels (this manuscript and ref *32*) and that Asn^{430}Ala and Leu^{346}Ala mutations significantly diminish channel expression. Therefore, this cluster of residues appears to be very critical for channel expression, and mutations in this region may cause significant structural changes in the pocket where diTC binds.

DISCUSSION

A major challenge in treatment of both graft rejection after a transplantation procedure, and autoimmune diseases, is the development of novel immunosuppressant agents with more limited toxicity profiles than the ones currently employed. The discovery that selective peptidyl blockers of the human T cell potassium channel, $K_v1.3$, inhibit Ca^{2+}-dependent processes of T cell activation has prompted the search for small molecules that display appropriate characteristics in terms of efficacy and tolerability. Correolide represents the first potent, small molecule, natural product inhibitor of $K_v1.3$ (*10*, *12*, *13*). Members of this family of compounds display immunosuppressant activity in in vivo models of T cell activation (*14*). In particular, these compounds have been shown to attenuate the delayed-type hypersensitivity reaction to tuberculin in the miniswine, and are well tolerated. Thus, it is important to understand the mechanism of correolide binding to $K_v1.3$ and to be able to use this information for developing more potent and selective inhibitors that have appropriate therapeutic efficacy, as well as enhanced safety margins. The goal of this work was the characterization, by site-directed mutagenesis, of the molecular determinants responsible for high affinity binding of diTC to $K_v1.3$. The results of these studies suggest that diTC binds in the water-filled cavity below the selectivity filter, and recognizes a complementary bowl-shape cavity formed by the side chains of specific S_6 residues. There is good experimental evidence to suggest that some of these residues are present in a region of the protein that changes conformation during gating (*32*). Although voltage-gated K^+ channels are highly conserved along S_6, C-type inactivation could confer a unique shape to the cavity where correolide binds in $K_v1.3$. In particular, members of the $K_v1.x$ family are 100% identical along S_5 and S_6, and the same residues that are critical for diTC binding to $K_v1.3$ appear also to be important for binding of diTC to $K_v1.2$. Since correolide interacts preferentially with the inactivated form of $K_v1.3$ (*13*, *14*), and kinetics of ligand binding correlate with the ease by which the channel enters the C-type inactivated state (*15*), the state-dependent interaction of members of the correolide family is consistent with the observed efficacy and limited toxicity of these compounds when tested in vivo.

Substitutions at Leu^{346} and Leu^{353} in S_5 and Ala^{413}, Val^{417}, Ala^{421}, Pro^{423}, and Val^{424} in S_6 cause the largest changes in the affinity of diTC for $K_v1.3$. In S_5, the two mutations are predicted to cause changes in the helical packing between S_5 and S_6 (Figure 5) which could lead to a change in the conformation of the diTC receptor. Thus, the lack of sensitivity of $K_v3.2$ to diTC is consistent with the presence of Phe in S_5 at the corresponding 346 position of $K_v1.3$, and it does not appear to reflect differences in the nature of the residues in the water cavity where diTC binds (*15*). Most of the critical residues of S_6 are expected to participate in the ligand binding site. Both Ala^{421} and Pro^{423} residues are conserved within voltage-gated channels. Ala^{421} is predicted to face the pore whereas Pro^{423} is on the opposite face away from the pore and close to Leu^{346} in S_5 (Figure 5). The results of different substitutions at Pro^{423} are also consistent with the idea that this residue affects diTC binding by determining the shape of the cavity through its packing with the S_5 helix, but it does not directly interact with the ligand. In the K_v2 family, Ile substitutes Val^{424}, but this substitution has no effect on diTC binding. It is interesting to note that in *Shaker*, the corresponding residues at positions Val^{424} and Pro^{425} display state-dependent reactivity toward sulfhydryl reagents when cysteines are substituted at these positions, suggesting that these residues are located at the boundary where gating-induced conformational changes occur (*32*). Several residues of S_6 with $\Delta\Delta G$ values of <1 kcal/mol such as Ile^{407}, Val^{408}, Ser^{410}, Leu^{411}, Ala^{415}, Tre^{419}, Val^{426}, and Ser^{429} are not conserved within voltage-gated potassium channels (*34*). This lack of sequence conservation correlates with the fact that, except for Val^{426} and Ser^{429}, the side chains of the corresponding residues in the KcsA channel face the lipid membrane.

Recent data suggest that in voltage-gated potassium channels, S_6 is not a continuous α-helical structure, and that these channels possess a bent structure at the P-V(I)-P region. The P-X-P sequence in these channels appears to behave as a flexible string connecting two alpha helical regions (*26*, *42*). Further support for this idea can be obtained from the results of the present study. It is obvious from the CPK models of Figure 3 that only the bent model can accommodate the experimental data. In this model, the intracellular entrance is wide open, and residues that have no impact on diTC binding are located far from the entranceway. The mutagenesis data at Pro^{423}, the first residue in the P-X-P region, further suggest that this residue is still part of the helix and that the kink may start at the second proline. Although alanine substitution at Pro^{423} causes a large effect on diTC binding, other substitutions such as Ile, Cys, Thr, and Asn are well tolerated, with Trp and Gln having an intermediate effect. Moreover, currents through Pro^{423}Ile channels have similar properties as those of $K_v1.3$ (data not shown), and the equivalent Pro^{423}Trp mutation in *Shaker* yields channels that gate, but do not conduct ionic current (*34*). If the kink in the S_6 helix would have occurred at Pro^{423}, it is likely that other residues would not have been well tolerated at this position. It does appear that the presence of Pro at position 423 of $K_v1.3$ is not absolutely required for proper gating/ion conduction of the channel and that the size of the residue at that position is a major determinant in diTC binding by affecting the shape of the cavity through its packing with the S_5 helix.

The effects of the Ala^{413}Cys mutant which greatly diminishes diTC binding are also of interest. The same mutation in *Shaker* decreases the apparent affinity of a potassium binding site in the pore, presumably by altering the interaction between the side chain of Ala^{463} in S_6 and the side chain of the potassium binding site, Val^{443}, in the pore (*33*). This mutation also decreases the rate of C-type inactivation in *Shaker* (*43*). These effects appear to reflect increased occupancy by potassium at the external C-type inactivation regulatory site due to diminished repulsive interactions between ions in the pore, as a result of the decrease in potassium affinity at the more internal site. The Ala^{413}Cys mutation in $K_v1.3$ also leads to a large decrease in the rate of C-type inactivation of the channel (data not shown). In addition, Ala^{413}Cys channels are insensitive to application of 1 μM correolide (data not shown). The effects of Ala^{413}-Cys could be similar to those of S_5 mutations and reflect a conformational change of the binding site.

These data, taken together, suggest that some of the residues that contribute to the high-affinity diTC receptor in $K_v1.3$ also play a role in defining some of the conformational transitions that occur during channel gating, and that the features that confer high affinity and specificity to the interaction of diTC with $K_v1.3$ are the result of events, such as C-type inactivation, that are not shared with most other voltage-gated K^+ channels. It is also possible that gating could be the result of conformational changes between the form of the channel illustrated in Figure 3A (closed state) and that of Figure 3B (open state). In Figure 3A, the channel does not present a favorable entrance way for correolide, and most residues at the entrance are of low impact for diTC binding. These features are consistent with the observation that correolide interacts with low affinity with the closed state of $K_v1.3$ (*13*). The conformational change induced in S_6 during gating through the P-X-P sequence could result in both channel opening and the formation of a high affinity site for correolide and its analogues (*13*, *14*). The P-X-P region could, therefore, be a major contributor to the gate of voltage-gated K^+ channels. It is important, however, to emphasize that the proposed models of Figure 3, and the docking model of diTC in Figure 4 are only a working hypothesis and will require more experimental data for their validation.

Other small molecule inhibitors of voltage-gated K^+ channels have also been identified. Among them, UK-78,-282 (*39*), WIN 17317−3 (*16*, *44*), and verapamil (*45*, *46*) have been shown to block $K_v1.3$ and inhibit T cell proliferation. Both UK-78,282 (*39*) and WIN 17317−3 (*16*) appear to interact with high affinity with C-type inactivated channels. A detailed characterization of the binding domains for these agents has not been carried out. However, inhibition of $K_v1.3$ by verapamil has been shown to be sensitive to mutation in one residue that is located in the region of the internal pore that forms part of the internal tetraethylamonium binding site (*38*), and the UK-78282 binding site appears to overlap with that of verapamil (*39*). Unfortunately, neither WIN 17317−3 nor verapamil are appropriate candidates for development as immunosuppressants because of the pronounced sodium channel blocking activity of WIN 17317−3 (*47*), and the calcium entry blocker properties of verapamil. Methanesulfonanilides, such as MK-499, bind with high affinity to C-type inactivated HERG potassium channels. The binding site is located within the water-filled cavity below the selectivity filter and contributed by three residues of S_6 and two of the pore helix (*48*). Thus, it appears that a common feature for some small molecules that block voltage-gated K^+ channels is to bind within this cavity. Selectivity among different classes of K^+ channels, such as $K_v1.x$ and HERG, can be derived from the differences in amino acid sequences of these proteins within such a common drug binding site. For example, correolide does not block HERG channels (6), and MK-499 does not block $K_v1.3$. Within a channel family, inhibitors can take advantage of specific characteristics of a given channel, such as C-type inactivation, to achieve a high affinity interaction. This state-dependent interaction should afford some channel specificity, independent of similarities in the primary amino acid sequence of the target proteins.

ACKNOWLEDGMENT

We thank Drs. Owen B. McManus, Richard Middleton, and Robert S. Slaughter for continuous discussions during the course of this work, and Drs. Brad Feuston and Robert Sheridan for their helpful discussions concerning modeling of the $K_v1.3$ channel.

REFERENCES

1. Kaczorowski, G., and Koo, G. C. (1994) *Perspect. Drug. Discuss. Des. 2*, 233.
2. Cahalan, M. D., and Chandy, K. G. (1997) *Curr. Opin. Biotechnol. 8*, 749−756.
3. Leonard, R. J., Garcia, M. L., Slaughter, R. S., and Reuben, J. P. (1992) *Proc. Natl. Acad. Sci. U.S.A. 89*, 10094−10098.
4. Helms, L. M. H., Felix, J. P., Bugianesi, R. M., Garcia, M. L., Stevens, S., Leonard, R. J., Knaus, H.-G., Koch, R.,

Wanner, S. G., Kaczorowski, G. J., and Slaughter, R. S. (1997) *Biochemistry 36*, 3737−3744.
5. Lin, C. S., Boltz, R. C., Blake, J. T., Nguyen, M., Talento, A., Fischer, P. A., Springer, M. S., Sigal, N. H., Slaughter, R. S., Garcia, M. L., Kaczorowski, G. J., and Koo, G. C. (1993) *J. Exp. Med. 177*, 637−645.
6. Price, M., Lee, S. C., and Deutsch, C. (1989) *Proc. Natl. Acad. Sci. U.S.A. 86*, 10171−10175.
7. Koo, G. C., Blake, J. T., Talento, A., Nguyen, M., Lin, S., Sirotina, A., Shah, K., Mulvany, K., Jr., D. H., Cunningham, P., Wunderler, D. L., McManus, O. B., Slaughter, R., Bugianesi, R., Felix, J., Garcia, M., Williamson, J., Kaczorowski, G., Sigal, N. H., Springer, M. S., and Feeney, W. (1997) *J. Immunol. 158*, 5120−5128.
8. Kalman, K., Pennington, M. W., Lanigan, M. D., Nguyen, A., Rauer, H., Mahnir, V., Paschetto, K., Kem, W. R., Grissmer, S., Gutman, G. A., Christian, E. P., Cahalan, M. D., Norton, R. S., and Chandy, K. G. (1998) *J. Biol. Chem. 273*, 32697−32707.
9. Beeton, C., Barbaria, J., Giraud, P., Devaux, J., Benoliel, A.-M., Gola, M., Sabatier, J. M., Bernard, D., Crest, M., and Beraud, E. (2001) *J. Immunol. 166*, 936−944.
10. Felix, J. P., Bugianesi, R. M., Schmalhofer, W. A., Borris, R., Goetz, M. A., Hensens, O. D., Bao, J.-M., Kayser, F., Parsons, W. H., Rupprecht, K., Garcia, M. L., Kaczorowski, G. J., and Slaughter, R. S. (1999) *Biochemistry 38*, 4922−4930.
11. Goetz, M. A., Hensens, O. D., Zink, D. L., Borris, R. P., Morales, F., Tamayo-Castillo, G., Slaughter, R. S., Felix, J., and Ball, R. G. (1998) *Tetrahedron Lett. 39*, 2895−2898.
12. Ghanshani, S., Wulff, H., Miller, M. J., Rohm, H., Neben, A., Gutman, G. A., Cahalan, M. D., and Chandy, K. G. (2000) *J. Biol. Chem. 275*, 37137−37149.
13. Wunderler, D., Leonard, R. J., Sanchez, M., and McManus, O. B. (1999) *Biophys. J. 76*, A186.
14. Koo, G. C., Blake, J. T., Shah, K., Staruch, M. J., Dumont, F., Wunderler, D., Sanchez, M., McManus, O. B., Sirotina-Meisher, A., Fischer, P., Boltz, R. C., Goetz, M. A., Baker, R., Bao, J., Kayser, F., Rupprecht, K. M., Parsons, W. H., Tong, X.-C., Ita, I. E., Pivnichny, J., Vincent, S., Cunningham, P., Jr., D. H., Feeney, W., Kaczorowski, G., and Springer, M. S. (1999) *Cell. Immunol. 197*, 99−107.
15. Hanner, M., Schmalhofer, W. A., Green, B., Bordallo, C., Liu, J., Slaughter, R. S., Kaczorowski, G. J., and Garcia, M. L. (1999) *J. Biol. Chem. 274*, 25237−25244.
16. Nguyen, A., Kath, J. C., Hanson, D. C., Biggers, M. S., Canniff, P. C., Donovan, C. B., Mather, R. J., Bruns, M. J., Rauer, H., Aiyar, J., Lepple-Wienhues, A., Gutman, G. A., Grissmer, S., Cahalan, M. D., and Chandy, K. G. (1996) *Mol. Pharmacol. 50*, 1672−1679.
17. Linde-Arias, A. R., Green, B., Matyskiela, M., Hanner, M., Schmalhofer, W. A., Kaczorowski, G. J., McManus, O. B., and Garcia, M. L. (2000) *Biophys. J. 78*, 212A.
18. Koschak, A., Bugianesi, R. M., Mitterdorfer, J., Kaczorowski, G. J., Garcia, M. L., and Knaus, H.-G. (1998) *J. Biol. Chem. 273*, 2639−2644.
19. Ho, S. N., Hunt, H. D., Horton, R. M., Pullen, J. K., and Pease, L. R. (1989) *Gene 77*, 51−59.
20. Hanner, M., Vianna-Jorge, R., Kamassah, A., Schmalhofer, W. A., Knaus, H.-G., Kaczorowski, G. J., and Garcia, M. L. (1998) *J. Biol. Chem. 273*, 16289−16296.
21. Doyle, D. A., Cabral, J. M., Pfuetzner, R. A., Kuo, A., Gulbis, J. M., Cohen, S. L., Chait, B. T., and MacKinnon, R. (1998) *Science 280*, 69−77.
22. Macarthur, M., and Thornton, J. M. (1991) *J. Mol. Biol. 218*, 397−412.
23. Williams, K. A., and Deber, C. M. (1991) *Biochemistry 30*, 8919−8923.
24. Javadpour, M. M., Eilers, M., Groesbeek, M., and Smith, S. O. (1999) *Biophys. J. 77*, 1609−1618.
25. Feuston, B. P., Miller, M. D., Culberson, J. C., Nachbar, R. B., and Kearsley, S. K. (2001) *J. Chem. Inf. Comput. Sci.* (in press).
26. Holmgren, M., Shin, K. S., and Yellen, G. (1998) *Neuron 21*, 617−621.
27. Shepard, W. E. B., Kingston, R. L., Anderson, B. F., and Baker, E. N. (1993) *Acta Crystallogr., Sect. D 49*, 331−343.
28. Brooks, B. R., Bruccoleri, R. E., Olafson, B. D., States, D. J., Swaminathan, S., and Karplus, M. (1983) *J. Comput. Chem. 4*, 187−217.
29. Halgren, T. A. (1999) *J. Comput. Chem. 20*, 720−729.
30. Crippen, G. M., and Havel, T. F. (1978) *Acta Crystallogr., Sect. A 34*, 282−284.
31. Miller, M. D., Kearsley, S. K., Underwood, D. J., and Sherida, R. P. (1994) *J. Comput. Aided Mol. Des. 8*, 153−174.
32. Liu, Y., Holmgren, M., Jurman, M. E., and Yellen, G. (1997) *Neuron 19*, 175−184.
33. Ogielska, E. M., and Aldrich, R. W. (1998) *J. Gen. Physiol. 112*, 243−257.
34. Li-Smerin, Y., Hackos, D. H., and Swartz, K. J. (2000) *Neuron 25*, 411−423.
35. Panyi, G., Sheng, Z. F., Tu, L. W., and Deutsch, C. (1995) *Biophys. J. 69*, 896−903.
36. Panyi, G., and Deutsch, C. (1996) *J. Gen. Physiol. 107*, 409−420.
37. Rauer, H., Lanigan, M. D., Pennington, M. W., Aiyar, J., Ghanshani, S., Cahalan, M. D., Norton, R. S., and Chandy, K. G. (2000) *J. Biol. Chem. 275*, 1201−1208.
38. Rauer, H., and Grissmer, S. (1999) *Br. J. Pharmacol. 127*, 1065−1074.
39. Hanson, D. C., Nguyen, A., Mather, R. J., Rauer, H., Koch, K., Burgess, L. E., Rizzi, J. P., Donovan, C. B., Bruns, M. J., Canniff, P. C., Cunningham, A. C., Verdries, K. A., Mena, E., Kath, J. C., Gutman, G. A., Cahalan, M. D., Grissmer, S., and Chandy, K. G. (1999) *Br. J. Pharmacol. 126*, 1707−1716.
40. Baker, R. K., Bao, J. M., Kayser, F., Parsons, W. H., and Rupprecht, K. (1998) U.S. Patent 5,679,705, Merck & Co., Inc.
41. Baker, R. K., Bao, J. M., Kayser, F., Parsons, W. H., and Rupprecht, K. (1998) U.S. Patent 5,679,156, Merck & Co., Inc.
42. Camino, D. d., Holgrem, M., Liu, Y., and Yellen, G. (2000) *Nature 403*, 321−325.
43. Ogielska, E. M., and Aldrich, R. W. (1999) *J. Gen. Physiol. 113*, 347−358.
44. Hill, R. J., Grant, A. M., Volberg, W., Rapp, L., Faltynek, C., Miller, D., Pagani, K., Baizman, E., Wang, S., Guiles, J. W., and Krafte, D. S. (1995) *Mol. Pharmacol. 48*, 98−104.
45. Chandy, K. G., DeCoursey, T. E., Cahalan, M. D., McLaughlin, C., and Gupta, S. (1984) *J. Exp. Med. 160*, 369−385.
46. Rauer, H., and Grissmer, S. (1996) *Mol. Pharmacol. 50*, 1625−1634.
47. Wanner, S. G., Glossman, H., Knaus, H.-G., Baker, R., Parsons, W., Rupprecht, K. M., Brochu, R., Cohen, C. J., Schmalhofer, W., Smith, M., Warren, V., Garcia, M. L., and Kaczorowski, G. J. (1999) *Biochemistry 38*, 11137−11146.
48. Mitcheson, J. S., Chen, J., Lin, M., Culberson, C., and Sanguinetti, M. C. (2000) *Proc. Natl. Acad. Sci. U.S.A. 97*, 12329−12333.

BI0111698